

MULTISCALE SCATTERED DATA ANALYSIS IN SAMPLET COORDINATES

SARA AVESANI, RÜDIGER KEMPF, MICHAEL MULTERER, AND HOLGER WENDLAND

ABSTRACT. We study multiscale scattered data interpolation schemes for globally supported radial basis functions, with a focus on the Matérn class. The multiscale approximation is constructed through a sequence of residual corrections, where radial basis functions with different lengthscale parameters are employed to capture varying levels of detail. To apply this approach to large data sets, we suggest to represent the resulting generalized Vandermonde matrices in samplet coordinates. Samplets are localized, discrete signed measures exhibiting vanishing moments and allow for the sparse approximation of generalized Vandermonde matrices issuing from a vast class of radial basis functions. Given a quasi-uniform set of N data sites, and local approximation spaces with geometrically decreasing dimension, the full multiscale system can be assembled with cost $\mathcal{O}(N \log N)$. We prove that the condition numbers of the linear systems at each level remain bounded independent of the particular level, allowing us to use an iterative solver with a bounded number of iterations for the numerical solution. Hence, the overall cost of the proposed approach is $\mathcal{O}(N \log N)$. The theoretical findings are accompanied by extensive numerical studies in two and three spatial dimensions.

1. INTRODUCTION

Interpolation using radial basis functions (RBFs) is a widely recognized technique for fitting functions based on scattered data in \mathbb{R}^d , see [10, 13, 14] for some surveys. RBF interpolation allows for the construction of approximation spaces in arbitrary dimensions and with varying levels of smoothness. These spaces are well known to provide high-quality approximations, see [11, 25]. However, the actual computation of an RBF interpolant usually entails a significant computational cost and the corresponding linear system is typically ill-conditioned. Even worse, as the convergence order increases, the associated problems become successively ill-conditioned. Moreover, using globally supported RBFs in interpolation leads to densely populated matrices, making the problem computationally infeasible for larger datasets. To address the latter, techniques such as interpolation using compactly supported RBFs have been developed [19, 24]. Unfortunately, even interpolation with these kernels becomes either computationally too expensive, if unscaled kernels are used, or do not even lead to convergence, if the support is scaled proportional to the fill-distance. Motivated by solving this trade-off principle, the works [3, 5, 9, 21], among many others, leverage the idea of a multiscale method where approximations on different scales are computed in an residual correction scheme. To date, the most general convergence theorems for multiscale interpolation using positive definite, compactly supported RBFs have been developed in [21]. The advantage of the multiscale method is that the condition numbers of the resulting linear systems at each level remain independent of the particular level. Thus achieving linear convergence in the number of used levels with relatively low cost.

In this article, we study the RBF interpolation problem using globally supported RBFs. We address the challenge of dealing with densely-populated interpolation matrices by employing *samplelet compression*, a technique introduced in [7]. Samplelets are discrete signed measures constructed such that all polynomials up to a certain degree vanish. This vanishing moment property allows for the compression of generalized Vandermonde matrices issuing from *asymptotically smooth* RBFs, i.e., they behave like smooth functions apart from zero. Hence, in samplelet coordinates, the resulting interpolation matrices become quasi-sparse, which means that they can be compressed such that only a sparse matrix remains. Furthermore, samplelets allow for a respective sparse matrix algebra, see [8], and provide a meaningful interpretation of sparsity constraints for scattered data, see [2]. However, as the samplelet transform of a given generalized Vandermonde matrix is an isometry up to the compression error, it does not alleviate the ill-conditioning. Therefore, to mitigate issues related to ill-conditioning, we adopt a multiscale interpolation approach that exploits scaled versions of the same RBF, which, in our case, remains globally supported. Hence, recovering the results from [21] for the class of Matérn kernels.

The remainder of this article is organized as follows. In Section 2, we revisit the classical multiscale interpolation algorithm, detailing the relevant subspaces and the class of radial basis functions considered in this work. In Section 3 we carry over a known result for compactly supported functions to globally supported RBFs: The condition number of the kernel matrix can be bounded uniformly in the number of sites, if we apply the appropriate scaling. Section 4 provides a brief introduction of samplelets, with a focus on the key properties of the basis transformation and compression. In Section 5, we present the multiscale interpolation algorithm within the samplelet basis and show an example of the resulting generalized Vandermonde matrix pattern. Finally, in Section 6, we provide numerical tests in both two and three spatial dimensions. Concluding remarks are stated in Section 7.

2. CLASSICAL MULTISCALE METHOD

Let $\Omega \subseteq \mathbb{R}^d$ be a domain and $X = \{\mathbf{x}_1, \dots, \mathbf{x}_N\} \subset \Omega$ be a set of data sites with cardinality $N = \#X$. Moreover, let $f \in C(\Omega)$ be the target function generating the data f_1, \dots, f_N . Associated to the set of sites X there are two measures, the *fill-distance* of X in Ω and the *separation radius* of X ,

$$h_{X,\Omega} := \sup_{\mathbf{x} \in \Omega} \min_{\mathbf{x} \in X} \|\mathbf{x} - \mathbf{x}_j\|_2$$

$$q_X := \frac{1}{2} \min_{j \neq k} \|\mathbf{x}_j - \mathbf{x}_k\|_2.$$

We call X *quasi-uniform* if there is a constant $c_{\text{qu}} > 0$ such that

$$q_X \leq h_{X,\Omega} \leq c_{\text{qu}} q_X.$$

Our goal is to interpolate or approximate the target function by means of *radial basis functions* (RBF) using only the given data $(\mathbf{x}_1, f_1), \dots, (\mathbf{x}_N, f_N)$. A function $\Phi: \mathbb{R}^d \rightarrow \mathbb{R}$ is said to be *radial*, if and only if there exists a univariate function $\phi: [0, \infty) \rightarrow \mathbb{R}$ such that $\Phi(\mathbf{x}) = \phi(\|\mathbf{x}\|_2)$. The radial function Φ is *strictly positive definite*, if and only if there holds for any choice of distinct points $\boldsymbol{\xi}_1, \dots, \boldsymbol{\xi}_n$, $n \in \mathbb{N}$, that

$$\boldsymbol{\alpha}^\top [\Phi(\boldsymbol{\xi}_i - \boldsymbol{\xi}_j)]_{i,j=1}^n \boldsymbol{\alpha} > 0 \quad \text{for all } \boldsymbol{\alpha} \in \mathbb{R}^n \setminus \{\mathbf{0}\}.$$

In this case, the kernel

$$K(\mathbf{x}_i, \mathbf{x}_j) := \Phi(\mathbf{x}_i - \mathbf{x}_j)$$

is the reproducing kernel of a uniquely determined reproducing kernel Hilbert space, its *native space*, that we denote by $(\mathcal{N}_\Phi, \langle \cdot, \cdot \rangle_{\mathcal{N}_\Phi})$. In this context, we will use the function Φ and its associated kernel K synonymously. A popular class of strictly positive RBFs are the *Matérn kernels* or *Sobolev splines* $\Phi_\nu: \mathbb{R}^d \rightarrow \mathbb{R}$, dependent on a hyper-parameter $\nu > d/2$. These kernels are defined via the radial function

$$(1) \quad \phi_\nu(r) = \frac{2^{1-\nu}}{\Gamma(\nu)} r^{\nu-\frac{d}{2}} K_{\nu-\frac{d}{2}}(r), \quad r \geq 0,$$

where Γ is the Riemann Gamma function and K_β is the modified Bessel function of the second kind, see [12] for example.

It is well-known that the Fourier transform of this radial function behaves like

$$(2) \quad \widehat{\Phi}(\boldsymbol{\omega}) = (1 + \|\boldsymbol{\omega}\|_2^2)^{-\nu-\frac{d}{2}}, \quad \boldsymbol{\omega} \in \mathbb{R}^d,$$

and that, in turn, the native space of the corresponding Matérn kernel is norm-equivalent to the classical Sobolev space $H^{\nu+\frac{d}{2}}(\mathbb{R}^d)$, see [20, Theorem 6.13] for example.

In this *instationary setting* it is known that the interpolant

$$s \in \mathcal{S} := \text{span}\{\Phi(\cdot - \mathbf{x}) : \mathbf{x} \in X\} \subset \mathcal{N}_\Phi$$

converges towards the target function f as $h_{X,\Omega} \rightarrow 0$. However, this improved approximation comes with higher and higher numerical cost for the iterative solution due to the ill-conditioning. To alleviate this cost, we can rescale the kernel, i.e., we introduce the parameter $\delta > 0$ and define

$$(3) \quad \Phi_\delta := \delta^{-d} \Phi\left(\frac{\cdot}{\delta}\right).$$

In the *stationary setting* we couple δ proportional to $h_{X,\Omega}$, i.e., there is a *coupling parameter* $\eta > 0$ such that $\delta = \eta h_{X,\Omega}$. In this case we can control the numerical costs to compute the interpolant but cannot expect convergence. This is known as the *trade-off principle*.

The idea of the multiscale method is now to introduce a hierarchy

$$(4) \quad X_1, X_2, \dots, X_L = X,$$

where we refer to the subscript of X_ℓ as level with cardinalities N_ℓ and fill-distances $h_\ell := h_{X_\ell,\Omega}$. Although in many applications the sets will be nested, for the multiscale method itself, this is not necessary. We assume that the cardinalities of the sets X_ℓ are increasing with the level, i.e., $N_\ell \leq N_{\ell+1}$ or, in other words, $h_\ell \geq h_{\ell+1}$. We quantify this relation in Theorem 2.1. Now, we use the stationary setting on each level ℓ . We have level-dependent $\delta_\ell > 0$ and level-dependently rescaled kernel K_ℓ given by

$$K_\ell(\mathbf{x}, \mathbf{y}) := \Phi_\ell(\mathbf{x} - \mathbf{y}) = \delta_\ell^{-d} \Phi\left(\frac{\mathbf{x} - \mathbf{y}}{\delta_\ell}\right), \quad \mathbf{x}, \mathbf{y} \in \mathbb{R}^d.$$

Each set X_ℓ in the multiscale hierarchy (4), together with the respective kernel, gives rise to a subspace

$$(5) \quad \mathcal{S}_\ell := \text{span}\{\Phi_\ell(\cdot - \mathbf{x}) : \mathbf{x} \in X_\ell\} \subset \mathcal{N}_{\Phi_\ell},$$

also called *local approximation space*.

With the multiscale sequence of points and the associated kernels, we can decompose the original approximation problem into L steps using a telescoping sum

$$\begin{aligned} s_1|_{X_1} &=: w_1|_{X_1} = f|_{X_1}, \\ w_2|_{X_2} &= (f - w_1)|_{X_2}, \\ &\vdots \\ w_L|_{X_L} &= \left(f - \sum_{\ell=1}^{L-1} w_\ell \right) \Big|_{X_L}. \end{aligned}$$

The intuition is that at the ℓ -th step we compute the approximation to the *error function* or *residual* of level $\ell - 1$, i.e.,

$$(6) \quad f - (w_1 + \cdots + w_{\ell-1})$$

in the space \mathcal{S}_ℓ , given as

$$(7) \quad w_\ell(\mathbf{x}) = \sum_{i=1}^{N_\ell} c_{\ell,i} \Phi_\ell(\mathbf{x} - \mathbf{x}_i), \quad \mathbf{x} \in \Omega,$$

with a coefficient vector $\mathbf{c}_\ell \in \mathbb{R}^{N_\ell}$.

From this, we obtain the multiscale decomposition

$$s_L := (w_1 + \cdots + w_L)|_X = f|_X,$$

which means that $s_L \in \cup_{\ell=1}^L \mathcal{S}_\ell$ matches f at each of the data sites in X .

In practice, the multiscale approximation process begins with a coarse set of points, where the approximation problem (7) is solved. Next, the error function (6) is computed, and finally, the latter is approximated at a finer scale. Interpolating the residual at level ℓ can be written in the following form:

$$\mathbf{K}_{\ell,\ell} \mathbf{c}_\ell = \mathbf{f}_\ell - \sum_{\ell'=1}^{\ell-1} \mathbf{K}_{\ell,\ell'} \mathbf{c}_{\ell'},$$

where

$$\mathbf{K}_{\ell,\ell'} := [\Phi_{\ell'}(\mathbf{x}_i^{(\ell)} - \mathbf{x}_j^{(\ell')})]_{i,j}, \quad \ell, \ell' = 1, \dots, L.$$

Therefore, the algorithm to solve the multiscale interpolation consists of solving the following triangular system, whose entries are matrices of different sizes:

$$(8) \quad \begin{bmatrix} \mathbf{K}_{1,1} & & & & \\ \mathbf{K}_{2,1} & \mathbf{K}_{2,2} & & & \\ \mathbf{K}_{3,1} & \mathbf{K}_{3,2} & \mathbf{K}_{3,3} & & \\ \vdots & \vdots & \cdots & \ddots & \\ \mathbf{K}_{L,1} & \mathbf{K}_{L,2} & \cdots & \mathbf{K}_{L,L-1} & \mathbf{K}_{L,L} \end{bmatrix} \begin{bmatrix} \mathbf{c}_1 \\ \mathbf{c}_2 \\ \mathbf{c}_3 \\ \vdots \\ \mathbf{c}_L \end{bmatrix} = \begin{bmatrix} \mathbf{f}_1 \\ \mathbf{f}_2 \\ \mathbf{f}_3 \\ \vdots \\ \mathbf{f}_L \end{bmatrix}$$

The resulting matrix is in general a densely-populated lower triangular matrix as a result of the choice of globally supported RBFs for the approximation at each level. The samplet compression plays a crucial role here, rendering the matrix quasi-sparse. This technique is introduced in Section 4, and the linear system is reformulated in the samplet basis in Section 5.

There holds the following convergence result, see, e.g., [21, 22].

Theorem 2.1. *Let $\Omega \subseteq \mathbb{R}^d$ be a bounded domain with Lipschitz boundary. Let X_1, X_2, \dots be a sequence of point sets in Ω with fill-distances h_1, h_2, \dots satisfying*

$$(9) \quad c\mu h_\ell \leq h_{\ell+1} \leq \mu h_\ell$$

for $\ell = 1, 2, \dots$ with fixed $\mu \in (0, 1)$, $c \in (0, 1]$ and h_1 sufficiently small. Let $\Phi: \mathbb{R}^d \rightarrow \mathbb{R}$ be a reproducing kernel for $H^s(\mathbb{R}^d)$, i.e., its Fourier transform satisfies

$$c_1(1 + \|\boldsymbol{\omega}\|_2^2)^{-s} \leq \widehat{\Phi}(\boldsymbol{\omega}) \leq c_2(1 + \|\boldsymbol{\omega}\|_2^2)^{-s}, \quad \boldsymbol{\omega} \in \mathbb{R}^d,$$

and let Φ_ℓ be the rescaled kernel as in (3) with scale factor $\delta_\ell = \eta h_\ell$, $\eta > 0$. Let $f \in H^s(\Omega)$. Then there exist constants C and $C_1 > 0$ such that

$$\|f - s_L\|_{L_2(\Omega)} \leq C(C_1\mu^s + C_1\eta^{-s})^L \|f\|_{H^s(\Omega)}.$$

3. CONDITION NUMBER BOUND FOR GENERALIZED VANDERMONDE MATRICES

We now show that the condition number cond_2 of the generalized Vandermonde matrix $\mathbf{K}_{\ell,\ell}$ of the scaled kernel can be bounded by a constant, independently of the level ℓ . A similar result in the context of the multiscale method for compactly supported RBFs has been derived in [18] using techniques of [15, 16]. We will reuse these techniques, with appropriate modifications. Furthermore, for a lighter notation, we will drop the subscripts ℓ in this section.

It goes without saying that, such a bound can not be established for general sets of sites X . Hence, for this section, we assume that X is quasi-uniform and the parameters of the multilevel method are chosen as in Theorem 2.1.

We remark that the algebraic decay of the Fourier transform of the Matérn kernel (2) immediately yields for the scaled RBF Φ_δ that

$$(10) \quad \widehat{\Phi}_\delta(\boldsymbol{\omega}) = (1 + \delta^2\|\boldsymbol{\omega}\|_2^2)^{-\nu - \frac{d}{2}}, \quad \boldsymbol{\omega} \in \mathbb{R}^d.$$

We will bound the smallest and largest eigenvalue of the matrix \mathbf{K} separately. We follow the ideas of [15, 16, 18].

Theorem 3.1. *Let $\Omega \subseteq \mathbb{R}^d$ be a bounded domain and $X \subseteq \Omega$ be a quasi-uniform set of sites with fill-distance $h_{X,\Omega}$ and separation radius q_X . Let Φ be the Matérn kernel and Let $\Phi_\delta = \delta^{-d}\Phi(\cdot/\delta)$ be the rescaled kernel where $\delta = \eta h_{X,\Omega}$ with overlap parameter $\eta > 1$. Then there exists a constant $C = C(\Phi, d, s)$ such that the bound for the smallest eigenvalue λ_{\min} of $\mathbf{K} = [\Phi_\delta(\mathbf{x}_i - \mathbf{x}_j)]_{i,j}$*

$$\lambda_{\min}(\mathbf{K}) \geq C(\eta c_{\text{qu}})^{d-2s} \delta^{-d}$$

holds. The largest eigenvalue of \mathbf{K} can be bounded from above by

$$\lambda_{\max}(\mathbf{K}) \leq \widetilde{C} \delta^{-d},$$

with a constant $\widetilde{C} = C(\Phi, d, \nu, \eta, c_{\text{qu}})$.

Proof. We set

$$\widetilde{\mathbf{K}} = \delta^d \mathbf{K} = \left[\Phi\left(\frac{\mathbf{x}_i - \mathbf{x}_j}{\delta}\right) \right]_{i,j}.$$

The lower bound follows immediately from [18, Proof of Proposition 3.4].

We only need to prove the upper bound for $\lambda_{\max}(\mathbf{K})$. We use Gershgorin's circle theorem, see, e.g. [23, Theorem 5.1] for $\widetilde{\mathbf{K}}$. Since the diagonal elements in this matrix are

$\Phi(\mathbf{0})$, independent of the line j , we can, without loss of generality, set $j = 1$ and $\mathbf{x}_1 = \mathbf{0}$. We have

$$(11) \quad |\lambda - \Phi(\mathbf{0})| \leq \sum_{k=2}^N \left| \Phi\left(\frac{\mathbf{0} - \mathbf{x}_k}{\delta}\right) \right| = \sum_{k=2}^N \left| \Phi\left(\frac{\mathbf{x}_k}{\delta}\right) \right|.$$

To bound the right hand side of this estimate, we introduce the annuli E_n given by

$$E_n = \{\mathbf{x} \in \mathbb{R}^d : nq_X \leq \|\mathbf{x}\|_2 < (n+1)q_X\}.$$

Each \mathbf{x}_k is contained in exactly one E_n and we can estimate

$$\#\{\mathbf{x}_k \in E_n\} \leq 3^d n^{d-1},$$

see, e.g., [20, Proof of Theorem 12.3]. Inserting this into (11) yields

$$(12) \quad \begin{aligned} |\lambda_{max}(\widetilde{\mathbf{K}}) - \Phi(\mathbf{0})| &\leq \sum_{k=2}^N \left| \Phi\left(\frac{\mathbf{x}_k}{\delta}\right) \right| \\ &\leq \sum_{n=1}^{\infty} \sum_{\mathbf{x}_k \in E_n} \left| \Phi\left(\frac{\mathbf{x}_k}{\delta}\right) \right| \\ &\leq \sum_{n=1}^{\infty} \#\{\mathbf{x}_k \in E_n\} \sup_{\mathbf{x} \in E_n} \left| \Phi\left(\frac{\mathbf{x}}{\delta}\right) \right|. \end{aligned}$$

Next, we bound $\sup_{\mathbf{x} \in E_n} |\Phi(\mathbf{x}/\delta)|$. We use the specific form of Φ , cp. (1), and the fact that the function $r \mapsto r^\beta K_\beta(r)$ is non-increasing on $(0, \infty)$ for any $\beta \in \mathbb{R}$, see [20, Corollary 5.12]. This yields

$$\begin{aligned} \frac{\Gamma(\nu)}{2^{1-\nu}} \sup_{\mathbf{x} \in E_n} \left| \Phi\left(\frac{\mathbf{x}}{\delta}\right) \right| &= \sup_{\mathbf{x} \in E_n} \left(\frac{\|\mathbf{x}\|_2}{\delta} \right)^{\nu - \frac{d}{2}} K_{\nu - \frac{d}{2}} \left(\frac{\|\mathbf{x}\|_2}{\delta} \right) \\ &\leq \left(\frac{nq_X}{\delta} \right)^{\nu - \frac{d}{2}} K_{\nu - \frac{d}{2}} \left(\frac{nq_X}{\delta} \right) \\ &\leq \left(\frac{nq_X}{\delta} \right)^{\nu - \frac{d}{2}} \sqrt{2\pi} \left(\frac{\delta}{nq_X} \right)^{\frac{1}{2}} \exp\left(-\frac{nq_X}{\delta}\right) \exp\left(\left(\nu - \frac{d}{2}\right)^2 \frac{2\delta}{2nq_X}\right), \end{aligned}$$

where we used the asymptotic behavior [20, Lemma 5.13] of the modified Bessel function to arrive at the last inequality. Inserting this into (12), using the quasi-uniformity of X and the coupling of δ to $h_{X,\Omega}$, as in Theorem 2.1, yields

$$\begin{aligned} |\lambda_{max}(\widetilde{\mathbf{K}}) - \Phi(\mathbf{0})| &\leq \sum_{n=1}^{\infty} \#\{\mathbf{x}_k \in E_n\} \sup_{\mathbf{x} \in E_n} \left| \Phi\left(\frac{\mathbf{x}}{\delta}\right) \right| \\ &\leq \sum_{n=1}^{\infty} 3^d n^{d-1} \sqrt{2\pi} \eta^{\frac{d}{2} - \nu} (\eta c_{qu})^{\frac{1}{2}} n^{\nu - \frac{d}{2} - \frac{1}{2}} \exp\left(-\frac{n}{\eta} + \frac{(\nu - \frac{d}{2})^2 \eta c_{qu}}{2n}\right) \\ &\leq \sqrt{2\pi} 3^d \eta^{\frac{d}{2} - \nu} (\eta c_{qu})^{\frac{1}{2}} \sum_{n=1}^{\infty} n^{\nu - \frac{d}{2} - \frac{3}{2}} \exp\left(-\frac{n}{\eta} + \frac{(\nu - \frac{d}{2})^2 \eta c_{qu}}{2n}\right). \end{aligned}$$

Since the series on the right hand side of the estimate converges, this yields the claimed bound for λ_{max} . \square

The derived bounds on λ_{min} and λ_{max} lead to the boundedness of the condition number of the generalized Vandermonde matrix for every level, uniformly in the number of data sites and the scaling parameter.

Corollary 3.2. *For every $\ell \in \mathbb{N}$ the condition number $\text{cond}_2(\mathbf{K}_{\ell,\ell})$ is bounded independently of N_ℓ and δ_ℓ .*

4. SAMPLETS FOR SCATTERED DATA APPROXIMATION

Samplets are discrete signed measures, which exhibit vanishing moments. We briefly recall their underlying concepts as introduced in [7]. To this end, we consider the image of the spaces \mathcal{S}_ℓ , $\ell = 1, \dots, L$, under the Riesz isomorphism $\mathcal{J}: \mathcal{N}_{\Phi_\ell} \rightarrow \mathcal{N}'_{\Phi_\ell}$ and define

$$(13) \quad \mathcal{S}'_\ell := \text{span}\{\mathcal{J}\Phi_\ell(\cdot - \mathbf{x}) : \mathbf{x} \in X_\ell\} = \text{span}\{\delta_{\mathbf{x}} : \mathbf{x} \in X_\ell\},$$

by the identity $\mathcal{J}\Phi_\ell(\cdot - \mathbf{x}) = \delta_{\mathbf{x}}$, where $\delta_{\mathbf{x}}$ is the point evaluation functional at $\mathbf{x} \in \Omega$. On the spaces \mathcal{S}'_ℓ , we introduce an inner product different from the canonical one by the defining property $\langle \delta_{\mathbf{x}_i}, \delta_{\mathbf{x}_j} \rangle_{\mathcal{S}'_\ell} := \delta_{ij}$ for $\mathbf{x}_i, \mathbf{x}_j \in X_\ell$.

For the sake of a more lightweight notation, we drop the subscript ℓ of the spaces \mathcal{S}'_ℓ for the remainder of this paragraph and remark that each space \mathcal{S}'_ℓ will in general have a different multiresolution analysis, where the maximum level J depends on ℓ . Given a multiresolution analysis

$$(14) \quad \mathcal{V}'_0 \subset \mathcal{V}'_1 \subset \dots \subset \mathcal{V}'_J = \mathcal{S}',$$

we keep track of the increment of information between two consecutive levels j and $j+1$. Since there holds $\mathcal{V}'_j \subset \mathcal{V}'_{j+1}$, we may orthogonally decompose

$$\mathcal{V}'_{j+1} = \mathcal{V}'_j \oplus \mathcal{W}'_j$$

for a certain *detail space* \mathcal{W}'_j . In analogy to wavelet nomenclature, we call the elements of a basis of \mathcal{V}'_0 *scaling distributions* and the elements of a basis of one of the spaces \mathcal{W}'_j *samplets*. This name is motivated by the idea that the basis distributions in \mathcal{W}'_j are supported at a small subsample or samplet of the data sites in X . The collection of the bases of \mathcal{W}'_j for $j = 0, \dots, J-1$ together with a basis of \mathcal{V}'_0 is called a *samplet basis* for \mathcal{S}' . A samplet basis can be constructed such that it exhibits *vanishing moments* of order $q+1$, i.e.,

$$(15) \quad (p, \sigma_{j,k})_\Omega = 0 \text{ for all } p \in \mathcal{P}_q,$$

where $\sigma_{j,k} \in \mathcal{W}'_j$ is a samplet and $\mathcal{P}_q := \text{span}\{\mathbf{x}^\alpha : \|\alpha\|_1 \leq q\}$ denotes the space of polynomials of total degree at most q .

The samplet construction for \mathcal{S}' is based on a *cluster tree* for the set of data sites X , i.e., a tree \mathcal{C} with root X such that each node $\tau \in \mathcal{C}$ is the disjoint union of its children. Such a cluster tree \mathcal{C} directly induces a support based hierarchical clustering of the subspace \mathcal{S}' , spanned by the Dirac- δ -distributions supported at the data sites in X . With a slight abuse of notation, we will refer to this cluster tree also by \mathcal{C} and to its elements by τ . Given a cluster tree \mathcal{C} , a samplet basis for \mathcal{S}' , where $\dim \mathcal{S}' = N$, can be constructed with cost $\mathcal{O}(N)$. Assuming furthermore, that \mathcal{C} is a balanced binary tree with maximum level $J = \lceil \log_2(N) \rceil$, the samplet basis exhibits the following properties, see [7] but also [6, 17].

Theorem 4.1. *The samplet basis $\bigcup_{j=0}^J \{\sigma_{j,k}\}_k$ forms an orthonormal basis in \mathcal{S}' , satisfying the following properties:*

- (1) *There holds $c^{-1}2^j \leq \dim \mathcal{W}'_j \leq c2^j$ for a constant $1 < c \leq 2$.*
- (2) *The samplets have vanishing moments of order $q+1$, i.e., $(p, \sigma_{j,k})_\Omega = 0$ for all $p \in \mathcal{P}_q(\Omega)$, where $\mathcal{P}_q(\Omega)$ is the space of polynomials up to degree q .*

(3) The coefficient vector $\boldsymbol{\omega}_{j,k} = [\omega_{j,k,i}]_i$ of the samplet $\sigma_{j,k}$ satisfies the bound

$$\|\boldsymbol{\omega}_{j,k}\|_1 \leq c2^{(J-j)/2}$$

for a constant $0 < c < 2$.

(4) Given $f \in C^{q+1}(O)$, for some open set $O \supset \text{supp } \sigma_{j,k}$, there holds

$$|\sigma_{j,k}(f)| \leq \left(\frac{d}{2}\right)^{q+1} \frac{(\text{diam } \text{supp } \sigma_{j,k})^{q+1}}{(q+1)!} \|f\|_{C^{q+1}(O)} \|\boldsymbol{\omega}_{j,k}\|_1.$$

(5) For quasi-uniform sets X , there holds $\text{diam } \text{supp } \sigma_{j,k} \leq c2^{-j/d}$ for some constant $c > 0$.

A direct consequence of the orthonormality of the samplet basis is that the samplet transform

$$[\sigma_{j,k}]_{j,k} = \mathbf{T}[\delta_{\mathbf{x}_i}]_{i=1}^N$$

satisfies $\mathbf{T}^\top \mathbf{T} = \mathbf{T} \mathbf{T}^\top = \mathbf{I} \in \mathbb{R}^{N \times N}$. If the samplet transform \mathbf{T} is computed recursively adhering the hierarchy induced by the cluster tree \mathcal{C} , its cost is of order $\mathcal{O}(N)$.

Employing the Riesz isometry, the samplet basis gives rise to a basis for $\mathcal{S} \subset \mathcal{N}_\Phi$. To this end, consider a samplet

$$\sigma_{j,k} = \sum_{i=1}^N \omega_{j,k,i} \delta_{\mathbf{x}_i}.$$

The samplet can be identified with the function

$$\psi_{j,k} := \sum_{i=1}^N \omega_{j,k,i} \Phi(\mathbf{x}_i - \cdot) \in \mathcal{S}$$

by means of the Riesz isometry. The vanishing moment property (15) then translates to

$$\langle \psi_{j,k}, f \rangle_{\mathcal{N}_\Phi} = 0$$

for any $f \in \mathcal{N}_\Phi$ which satisfies $f|_O \in \mathcal{P}_q$ for any open and convex set O with $\text{supp}(\sigma_{j,k}) \subset O \cap \Omega$.

Furthermore, there holds

$$(16) \quad \left[\langle \psi_{j,k}, \psi_{j',k'} \rangle_{\mathcal{N}_\Phi} \right]_{j,j',k,k'} = \mathbf{T} \mathbf{K} \mathbf{T}^\top =: \mathbf{K}^\Sigma.$$

This means that the Gramian of the embedded samplet basis in \mathcal{S} is just the samplet transformed generalized Vandermonde matrix. For *asymptotically smooth* kernels K , i.e. that there exist $C, r > 0$ such that for all $(\mathbf{x}, \mathbf{y}) \in (\Omega \times \Omega) \setminus \Delta$

$$(17) \quad \left| \frac{\partial^{|\boldsymbol{\alpha}|+|\boldsymbol{\beta}|}}{\partial \mathbf{x}^\alpha \partial \mathbf{y}^\beta} K(\mathbf{x}, \mathbf{y}) \right| \leq C \frac{(|\boldsymbol{\alpha}| + |\boldsymbol{\beta}|)!}{r^{|\boldsymbol{\alpha}|+|\boldsymbol{\beta}|} \|\mathbf{x} - \mathbf{y}\|_2^{|\boldsymbol{\alpha}|+|\boldsymbol{\beta}|}}$$

uniformly in $\boldsymbol{\alpha}, \boldsymbol{\beta} \in \mathbb{N}^d$ apart from the diagonal $\Delta := \{(\mathbf{x}, \mathbf{y}) \in \Omega \times \Omega : \mathbf{x} = \mathbf{y}\}$, the matrix \mathbf{K}^Σ becomes quasi-sparse and can efficiently be computed. More precisely, there holds the following result, see [7].

Theorem 4.2. *Let X be quasi-uniform with $\#X = N$ and set all coefficients of the generalized Vandermonde matrix \mathbf{K}^Σ from (16) to zero which satisfy the admissibility condition*

$$(18) \quad \text{dist}(\tau, \tau') \geq \rho \max\{\text{diam}(\tau), \text{diam}(\tau')\}, \quad \rho > 0,$$

where τ is the cluster supporting $\sigma_{j,k}$ and τ' is the cluster supporting $\sigma_{j',k'}$, respectively. Then, there exists a constant $C > 0$, such that

$$(19) \quad \frac{\|\mathbf{K}^\Sigma - \mathbf{K}_\varepsilon^\Sigma\|_F}{\|\mathbf{K}^\Sigma\|_F} \leq Cm_q(r\rho/d)^{-2(q+1)},$$

where $m_q = \binom{q+d}{d}$ is the dimension of \mathcal{P}_q , and the compressed matrix has $\mathcal{O}(m_q^2 N \log N)$ nonzero coefficients.

5. MULTISCALE ALGORITHM IN SAMPLET COORDINATES

In this section, we transform the interpolation problem from the original basis, referred to as the *natural basis*, to the samplet basis, which consists of the scaling distributions and the samplets, as introduced in Section 4. In what follows, we denote the samplet transform for \mathcal{S}'_ℓ by $\mathbf{T}_\ell \in \mathbb{R}^{N_\ell \times N_\ell}$ and recall that $\mathbf{T}_\ell^\top \mathbf{T}_\ell = \mathbf{T}_\ell \mathbf{T}_\ell^\top = \mathbf{I} \in \mathbb{R}^{N_\ell \times N_\ell}$. Defining the block transform

$$(20) \quad \mathcal{T} := \begin{bmatrix} \mathbf{T}_1 & & & \\ & \mathbf{T}_2 & & \\ & & \ddots & \\ & & & \mathbf{T}_L \end{bmatrix},$$

there holds $\mathcal{T}^\top \mathcal{T} = \mathcal{T} \mathcal{T}^\top = \mathbf{I}$. Hence, the linear system (8) is equivalent to

$$\mathcal{T}^\top \mathcal{T} \begin{bmatrix} \mathbf{K}_{1,1} & & & \\ \mathbf{K}_{2,1} & \mathbf{K}_{2,2} & & \\ \vdots & \cdots & \ddots & \\ \mathbf{K}_{L,1} & \cdots & \mathbf{K}_{L,L-1} & \mathbf{K}_{L,L} \end{bmatrix} \mathcal{T}^\top \mathcal{T} \begin{bmatrix} \mathbf{c}_1 \\ \mathbf{c}_2 \\ \mathbf{c}_3 \\ \vdots \\ \mathbf{c}_L \end{bmatrix} = \mathcal{T}^\top \mathcal{T} \begin{bmatrix} \mathbf{f}_1 \\ \mathbf{f}_2 \\ \mathbf{f}_3 \\ \vdots \\ \mathbf{f}_L \end{bmatrix}$$

Letting $\mathbf{K}_{\ell,\ell'}^\Sigma := \mathbf{T}_\ell \mathbf{K}_{\ell,\ell'} \mathbf{T}_{\ell'}^\top$, $\mathbf{c}_\ell^\Sigma := \mathbf{T}_\ell \mathbf{c}_\ell$ and $\mathbf{f}_\ell^\Sigma := \mathbf{T}_\ell \mathbf{f}_\ell$ and dropping the inverse block transform, we arrive at the samplet transformed system

$$(21) \quad \begin{bmatrix} \mathbf{K}_{1,1}^\Sigma & & & & \\ \mathbf{K}_{2,1}^\Sigma & \mathbf{K}_{2,2}^\Sigma & & & \\ \mathbf{K}_1^{\Sigma,3} & \mathbf{K}_{3,2}^\Sigma & \mathbf{K}_{3,3}^\Sigma & & \\ \vdots & \vdots & \cdots & \ddots & \\ \mathbf{K}_{L,1}^\Sigma & \mathbf{K}_{L,2}^\Sigma & \cdots & \mathbf{K}_{L,L-1}^\Sigma & \mathbf{K}_{L,L}^\Sigma \end{bmatrix} \begin{bmatrix} \mathbf{c}_1^\Sigma \\ \mathbf{c}_2^\Sigma \\ \mathbf{c}_3^\Sigma \\ \vdots \\ \mathbf{c}_L^\Sigma \end{bmatrix} = \begin{bmatrix} \mathbf{f}_1^\Sigma \\ \mathbf{f}_2^\Sigma \\ \mathbf{f}_3^\Sigma \\ \vdots \\ \mathbf{f}_L^\Sigma \end{bmatrix},$$

which is equivalent to (8). In particular, since \mathcal{T} is an isometry, the condition number of the system (21) is identical to that of (8).

Furthermore, we remark that, for a geometric sequence $\{N_\ell\}_\ell$, the cost for applying \mathcal{T} and \mathcal{T}^\top , respectively, remains linear in N_L . Each block $\mathbf{K}_{\ell,\ell'}^\Sigma$, $\ell \leq \ell'$, can be computed with cost $\mathcal{O}(N_{\ell'} + N_\ell \log N_\ell)$ if $\{N_\ell\}_\ell$ forms a geometric sequence, cp. [1, Proof of Theorem 3.16]. Moreover, there are $\mathcal{O}(\log N_{\ell'})$ blocks per row, resulting in a computational cost of $\mathcal{O}(N_{\ell'} \log N_{\ell'})$ per row by the geometric sequence property of $\{N_\ell\}_\ell$. Summing up the cost for each row, exploiting the geometric sequence again, the overall computation cost for the assembly of the linear system (21) is bounded by $\mathcal{O}(N_L \log N_L)$. To give an idea of the sparsity pattern of the samplet compressed system (21), Figure 1 visualizes the matrix pattern $\mathbf{K}_{\ell,\ell'}^\Sigma$ using three levels of points X_1, X_2, X_3 arranged on a regular grid for the unit square, with cardinalities of 4 225, 66 049, and 1 050 625, respectively.

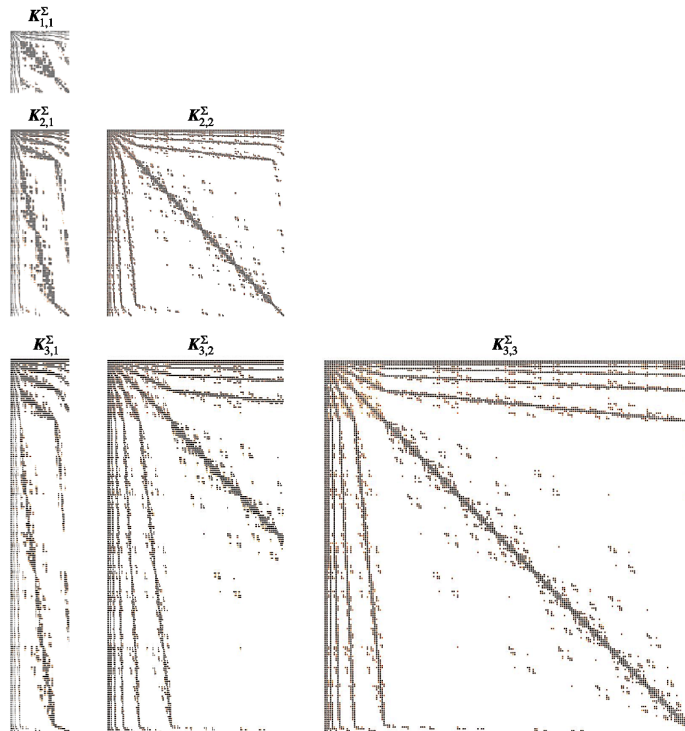


FIGURE 1. Example of the sparsity patterns of the matrices $\mathbf{K}_{\ell,\ell'}^\Sigma$ for $\ell, \ell' \in \{1, 2, 3\}$ in the linear system (21).

6. NUMERICAL RESULTS

We present numerical examples of the proposed multiscale interpolation in samplers coordinates in both two and three dimensional settings. The parameters for the sampler compression are ρ , q , and κ . The parameter ρ corresponds to the admissibility condition (18), which steers the a-priorily truncated matrix blocks. A larger ρ results in a larger distance between clusters before they are admissible for compression. In our analysis, we adopt $\rho = d$, so that the bound in Equation (19) is exponentially governed by the number of vanishing moments. This number of vanishing moments corresponds to $q+1$, as specified in (15). The higher q , the more polynomial exactness is gained. Lastly, κ serves as an a-posteriori compression threshold. After applying the sampler transform to the generalized Vandermonde matrix, we truncate entries smaller than κ , resulting in a sparser matrix representation.

To measure the approximation quality, we consider the relative interpolation errors

$$\text{error}_{p,\ell} = \frac{\|f - s_\ell\|_p}{\|f\|_p}$$

for $p = 2$ and $p = \infty$ at each of the levels $\ell = 1, \dots, L$. Furthermore, we compute the order of convergence, given by

$$\text{order}_{p,\ell} = \frac{\log\left(\frac{\text{error}_{p,\ell+1}}{\text{error}_{p,\ell}}\right)}{\log\left(\frac{h_{\ell+1}}{h_\ell}\right)}.$$

We investigate three different scenarios in our numerical tests. The first two are adapted from [21]: a smooth function on the unit square and a non-smooth function on the L-shaped

domain. Finally, we extend to a three dimensional setting issuing from the Lucy surface model of the `Stanford 3D Scanning Repository`¹.

All computations have been performed at the Centro Svizzero di Calcolo Scientifico (CSCS) on a single node of the Alps cluster² with two AMD EPYC 7742 @2.25GHz CPUs, up to 420GB of main memory and up to 20 cores. The implementation of the samplet compression is available as software package `FMCA`³.

6.1. Franke’s function in two spatial dimensions. We interpolate Franke’s function, as introduced in [4], defined by

$$(22) \quad f(x, y) = \frac{3}{4} \exp\left(-\frac{(9x-2)^2}{4} - \frac{(9y-2)^2}{4}\right) + \frac{3}{4} \exp\left(-\frac{(9x+1)^2}{49} - \frac{(9y+1)^2}{10}\right) \\ + \frac{1}{2} \exp\left(-\frac{(9x-7)^2}{4} - \frac{(9y-3)^2}{4}\right) - \frac{1}{5} \exp(-(9x-4)^2 - (9y-7)^2)$$

on the unit square $\Omega = [0, 1]^2$. To this end, we generate 10 sets of nested points within this domain, distributing them on a regular grid with size $h_j = 2^{-j}$. The number of points per level and the corresponding fill-distances are provided in Table 1.

ℓ	N_ℓ	h
1	9	0.5
2	25	0.25
3	81	0.125
4	289	0.0625
5	1 089	0.03125
6	4 225	0.015625
7	16 641	0.0078125
8	66 049	0.00390625
9	263 169	0.00195312
10	1 050 625	0.000976562

TABLE 1. Number of points per level and the corresponding fill-distances on $\Omega = [0, 1]^2$ for the interpolation of Franke’s function.

We have conducted computations using a-posteriori compression thresholds of $\kappa = 10^{-4}, 10^{-6}, 10^{-8}$. For $\kappa = 10^{-4}$, the error remains larger than 10^{-6} , due to an increased compression error. Setting $\kappa = 10^{-6}$, we have achieved an error of the order of 10^{-8} . Further reducing the threshold to $\kappa = 10^{-8}$ results in an error of 10^{-9} . Even so, the latter results in a significantly worse compression rate of the generalized Vandermonde matrices.

Therefore, we detail the results using $\kappa = 10^{-6}$ for the threshold. We approximate the solution with the C^1 -smooth Matérn-3/2 RBF and the C^2 -smooth Matérn-5/2 RBF and different values of γ . The error is evaluated at a fine grid with mesh-size $h = 2^{-11}$. The accuracy of the conjugate gradient method is set to 10^{-6} . Increasing the accuracy does not result in smaller errors but increases the number of iterations. Interpolation error, order and compression rate (%nz) as well as (non-preconditioned) conjugate gradient iterations (CG) are presented in the Tables 2 – 5.

¹<https://graphics.stanford.edu/data/3Dscanrep/>

²<https://www.cscs.ch/computers/alps>

³<https://github.com/muchip/fmca>

Matérn-3/2 RBF								
$\gamma = 0.25$					$\gamma = 0.5$			
ℓ	error ₂	order ₂	%nz	CG	error ₂	order ₂	%nz	CG
1	$5.67 \cdot 10^{-1}$	–	55	5	$4.84 \cdot 10^{-1}$	–	55	6
2	$1.38 \cdot 10^{-1}$	2.04	36	8	$5.29 \cdot 10^{-2}$	2.19	36	13
3	$3.16 \cdot 10^{-2}$	2.12	43	9	$9.20 \cdot 10^{-3}$	2.53	43	25
4	$6.76 \cdot 10^{-3}$	2.23	47	10	$1.15 \cdot 10^{-3}$	3.00	47	34
5	$1.48 \cdot 10^{-3}$	2.19	22	10	$2.51 \cdot 10^{-4}$	2.53	22	39
6	$3.45 \cdot 10^{-4}$	2.10	7.8	10	$6.08 \cdot 10^{-5}$	2.05	7.6	39
7	$8.30 \cdot 10^{-5}$	2.06	2.3	10	$1.30 \cdot 10^{-5}$	2.22	2.3	39
8	$1.46 \cdot 10^{-5}$	2.51	0.62	10	$1.14 \cdot 10^{-6}$	3.51	0.62	39
9	$3.14 \cdot 10^{-6}$	2.22	0.16	10	$1.04 \cdot 10^{-7}$	3.45	0.16	39
10	$7.89 \cdot 10^{-7}$	1.99	0.04	10	$4.47 \cdot 10^{-8}$	1.21	0.04	39

TABLE 2. Results for the interpolation of Franke’s function using the C^1 -smooth Matérn-3/2 RBF and $\rho = 2$, $q + 1 = 5$, $\kappa = 10^{-6}$ as samplet compression parameters.

Matérn-3/2 RBF								
$\gamma = 0.75$					$\gamma = 1$			
ℓ	error ₂	order ₂	%nz	CG	error ₂	order ₂	%nz	CG
1	$4.84 \cdot 10^{-1}$	–	55	6	$4.88 \cdot 10^{-1}$	–	55	6
2	$4.67 \cdot 10^{-2}$	3.37	36	17	$4.51 \cdot 10^{-2}$	3.43	36	20
3	$7.97 \cdot 10^{-3}$	2.55	43	41	$7.72 \cdot 10^{-3}$	2.55	43	48
4	$5.70 \cdot 10^{-4}$	3.81	47	64	$3.60 \cdot 10^{-4}$	4.43	47	97
5	$1.09 \cdot 10^{-4}$	2.38	23	90	$5.75 \cdot 10^{-5}$	3.31	25	156
6	$2.38 \cdot 10^{-5}$	2.19	8.2	96	$1.16 \cdot 10^{-5}$	2.31	8.9	187
7	$4.57 \cdot 10^{-6}$	2.38	2.5	98	$2.07 \cdot 10^{-6}$	2.82	2.7	195
8	$4.77 \cdot 10^{-7}$	3.26	0.68	99	$2.27 \cdot 10^{-7}$	3.19	0.74	197
9	$5.97 \cdot 10^{-8}$	3.00	0.18	99	$7.85 \cdot 10^{-8}$	1.53	0.19	199
10	$4.63 \cdot 10^{-8}$	0.37	0.05	99	$7.30 \cdot 10^{-8}$	0.10	0.05	200

TABLE 3. Results for the interpolation of Franke’s function using the C^1 -smooth Matérn-3/2 RBF and $\rho = 2$, $q + 1 = 5$, $\kappa = 10^{-6}$ as samplet compression parameters.

The tables clearly demonstrate the expected exponential decay of the approximation error with increasing level for both error measures and both RBFs under consideration. Furthermore, we see the effect of a larger value of γ , which to a greater lengthscale parameter of the RBF, resulting in a larger condition number. For increasing γ , we require successively more iterations for the conjugate gradient method to achieve the prescribed accuracy, with up to 430 iterations for $\gamma = 1$ and the Matérn-5/2 RBF. The deterioration of the convergence for $\gamma = 0.75, 1$ on the last level is caused by the samplet compression error, which is a directly to the chosen compression threshold κ .

Figure 2 shows a visualization of the solution (left) and the residuals (right) at levels $\ell = 1, 4, 7, 10$ for $\gamma = 1$ using the Matérn-3/2 RBF.

Matérn-5/2 RBF								
$\gamma = 0.25$					$\gamma = 0.5$			
ℓ	error ₂	order ₂	%nz	CG	error ₂	order ₂	%nz	CG
1	$5.45 \cdot 10^{-1}$	–	55	5	$4.72 \cdot 10^{-1}$	–	55	6
2	$1.12 \cdot 10^{-1}$	2.28	36	8	$4.51 \cdot 10^{-2}$	1.39	36	16
3	$2.27 \cdot 10^{-2}$	2.14	43	9	$7.73 \cdot 10^{-3}$	2.54	43	32
4	$4.54 \cdot 10^{-3}$	2.32	47	10	$6.92 \cdot 10^{-4}$	3.48	47	42
5	$1.00 \cdot 10^{-3}$	2.18	22	10	$1.49 \cdot 10^{-4}$	2.88	22	48
6	$2.49 \cdot 10^{-4}$	2.01	7.6	10	$3.42 \cdot 10^{-5}$	2.12	7.7	48
7	$6.13 \cdot 10^{-5}$	2.02	2.3	10	$6.88 \cdot 10^{-6}$	2.32	2.3	48
8	$6.06 \cdot 10^{-6}$	3.34	0.62	9	$8.31 \cdot 10^{-7}$	3.05	0.62	48
9	$1.15 \cdot 10^{-6}$	2.40	0.16	9	$6.15 \cdot 10^{-8}$	3.76	0.16	48
10	$3.07 \cdot 10^{-7}$	1.91	0.04	9	$1.57 \cdot 10^{-8}$	1.97	0.04	48

TABLE 4. Results for the interpolation of Franke’s function using the C^2 -smooth Matérn-5/2 RBF and $\rho = 2$, $q + 1 = 5$, $\kappa = 10^{-6}$ as samplelet compression parameters.

Matérn-5/2 RBF								
$\gamma = 0.75$					$\gamma = 1$			
ℓ	error ₂	order ₂	%nz	CG	error ₂	order ₂	%nz	CG
1	$4.79 \cdot 10^{-1}$	–	55	6	$9.16 \cdot 10^{-1}$	–	55	7
2	$4.41 \cdot 10^{-2}$	3.44	36	20	$4.69 \cdot 10^{-2}$	4.29	36	25
3	$7.13 \cdot 10^{-3}$	2.63	43	57	$7.47 \cdot 10^{-3}$	2.65	43	82
4	$3.29 \cdot 10^{-4}$	4.43	47	97	$1.63 \cdot 10^{-4}$	2.19	47	172
5	$6.14 \cdot 10^{-5}$	2.42	23	139	$3.96 \cdot 10^{-5}$	2.04	24	298
6	$1.22 \cdot 10^{-5}$	2.33	8.0	151	$1.34 \cdot 10^{-5}$	1.56	8.8	370
7	$2.11 \cdot 10^{-6}$	2.53	2.4	157	$2.06 \cdot 10^{-6}$	2.70	2.7	402
8	$2.57 \cdot 10^{-7}$	3.03	0.70	159	$2.39 \cdot 10^{-7}$	3.10	0.73	416
9	$4.06 \cdot 10^{-8}$	2.66	0.17	161	$7.56 \cdot 10^{-8}$	1.66	0.19	430
10	$3.04 \cdot 10^{-8}$	0.42	0.04	162	$7.01 \cdot 10^{-8}$	0.11	0.05	430

TABLE 5. Results for the interpolation of Franke’s function using the C^2 -smooth Matérn-5/2 RBF and $\rho = 2$, $q + 1 = 5$, $\kappa = 10^{-6}$ as samplelet compression parameters.

6.2. Non-smooth function. We consider the L-shaped domain $\Omega = [-\frac{1}{2}, \frac{1}{2}]^2 \setminus (0, \frac{1}{2}]^2$ where we introduce polar coordinates $x = r \cos \phi$, $y = r \sin \phi$, with $r \geq 0$ and $\phi \in [\pi/2, 2\pi]$. In this test, we aim at interpolating the function

$$u(r, \phi) = -r^{\frac{2}{3}} \sin\left(\frac{2\phi - \pi}{3}\right),$$

which solves the Laplace equation $\Delta u = 0$. We select $h_j = 2^{-j}$ as before. Given the reduced smoothness of the function, we choose the C^0 -smooth Matérn-1/2 RBF for its approximation. The error is evaluated at a fine grid with mesh-size $h = 2^{-9}$ and the accuracy of the conjugate gradient method is set to 10^{-6} .

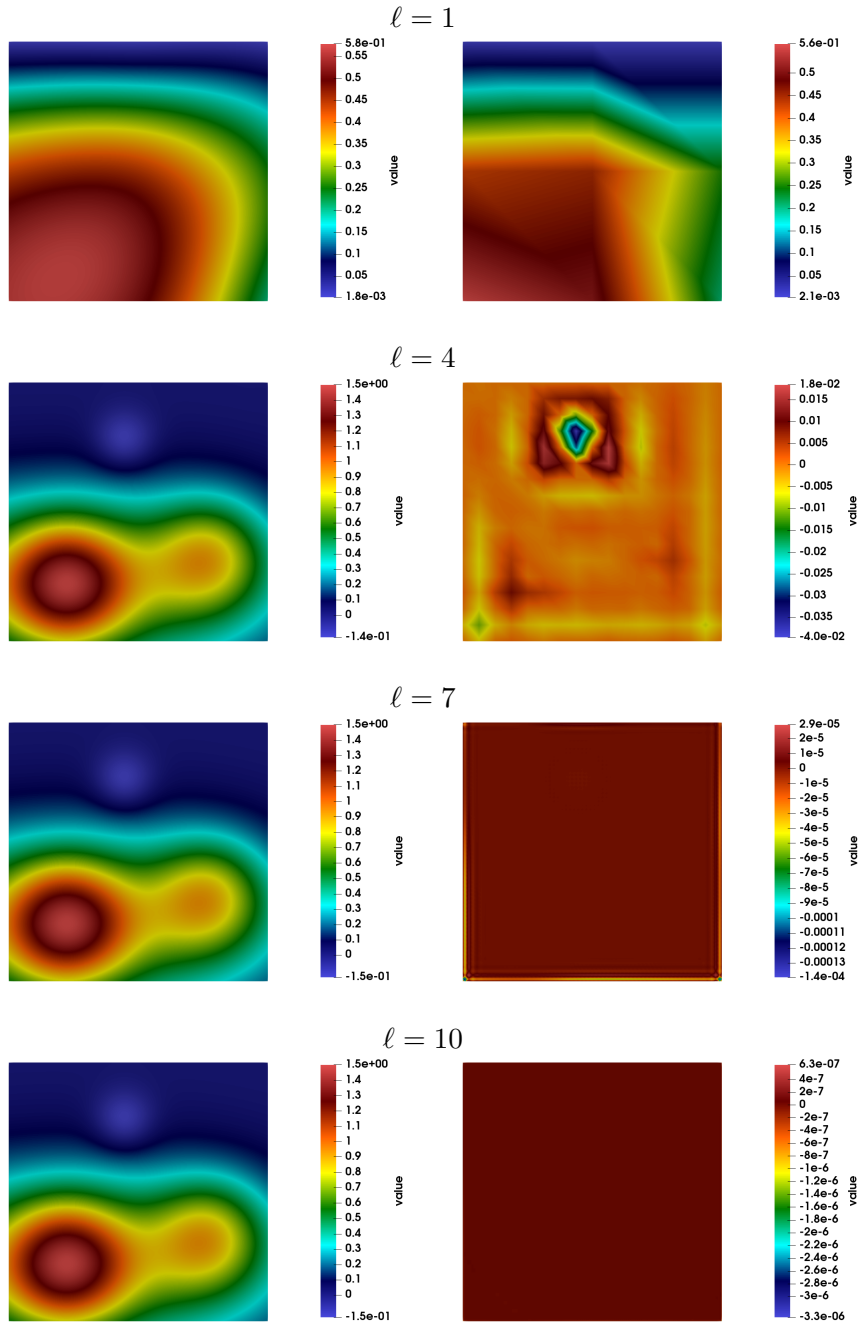


FIGURE 2. Solution (left) and corresponding residuals (right) for the interpolation of Franke's function for levels $\ell = 1, 4, 7, 10$.

We have conducted experiments using $\kappa = 10^{-4}, 10^{-6}, 10^{-8}$. While the magnitude of the errors remained consistent across these values, the compression rate in the final level increased as κ decreased. Specifically for $\kappa = 10^{-4}$, the compression rate is around 0.13%, for $\kappa = 10^{-6}$, it is about 0.30% and for $\kappa = 10^{-8}$ it is approximately 0.43%. Consequently, we chose a higher threshold to reduce computational cost and storage. The number of points per level and the corresponding fill-distances are provided in Table 6.

The results for $\gamma = 0.5$ and $\gamma = 1$ are summarized in Table 7.

ℓ	N_ℓ	h
1	21	0.25
2	65	0.125
3	225	0.0625
4	833	0.03125
5	3 201	0.015625
6	12 545	0.0078125
7	49 665	0.00390625
8	197 633	0.00195312

TABLE 6. Number of points per level and the corresponding fill-distances on the L-shaped domain for the interpolation of the solution to the Laplace equation.

$\gamma = 0.5$						
ℓ	error ₂	error _∞	order ₂	order _∞	%nz	CG
1	$4.37 \cdot 10^{-2}$	$5.98 \cdot 10^{-2}$	–	–	52	9
2	$1.38 \cdot 10^{-2}$	$3.17 \cdot 10^{-2}$	1.67	0.92	49	21
3	$5.33 \cdot 10^{-3}$	$2.04 \cdot 10^{-2}$	1.37	0.64	38	28
4	$1.83 \cdot 10^{-3}$	$1.29 \cdot 10^{-2}$	1.54	0.66	18	34
5	$5.88 \cdot 10^{-4}$	$8.15 \cdot 10^{-3}$	1.64	0.67	6.2	36
6	$1.85 \cdot 10^{-4}$	$5.04 \cdot 10^{-3}$	1.67	0.69	1.8	37
7	$5.87 \cdot 10^{-5}$	$3.11 \cdot 10^{-3}$	1.66	0.70	0.51	37
8	$1.89 \cdot 10^{-5}$	$1.61 \cdot 10^{-3}$	1.63	0.95	0.13	37

$\gamma = 1$						
ℓ	error ₂	error _∞	order ₂	order _∞	%nz	CG
1	$3.39 \cdot 10^{-2}$	$6.06 \cdot 10^{-2}$	–	–	48	13
2	$1.27 \cdot 10^{-2}$	$3.94 \cdot 10^{-2}$	1.41	0.62	49	28
3	$4.15 \cdot 10^{-3}$	$2.50 \cdot 10^{-2}$	1.62	0.66	37	49
4	$1.29 \cdot 10^{-3}$	$1.58 \cdot 10^{-2}$	1.68	0.66	18	73
5	$3.97 \cdot 10^{-4}$	$9.94 \cdot 10^{-3}$	1.70	0.67	6.0	93
6	$1.23 \cdot 10^{-4}$	$6.13 \cdot 10^{-3}$	1.70	0.70	1.8	102
7	$3.83 \cdot 10^{-5}$	$3.72 \cdot 10^{-3}$	1.68	0.72	0.12	104
8	$1.20 \cdot 10^{-5}$	$1.95 \cdot 10^{-3}$	1.68	0.76	0.09	105

TABLE 7. Results for the interpolation of the solution of the Laplace equation on the L-shaped domain using the C^0 -smooth Matérn-1/2 RBF and $\rho = 2$, $q + 1 = 5$, $\kappa = 10^{-4}$ as samplelet compression parameters.

The compression rates are similar to the previous example, also in case of the less smooth Matérn-1/2 RBF. The approximation error and the corresponding order are reduced, however. The number of conjugate gradient iterations stays rather low with a maximum of 37 iterations for $\gamma = 0.5$ and of 105 iterations for $\gamma = 1$. This can be explained by the slower decay of the Matérn-1/2 kernel's eigenvalues, resulting in less ill-conditioned generalized Vandermonde matrices.

Figure 3 illustrates the solution (left) and the corresponding residuals (right) at levels $\ell = 2, 4, 6, 8$ with $\gamma = 0.5$.

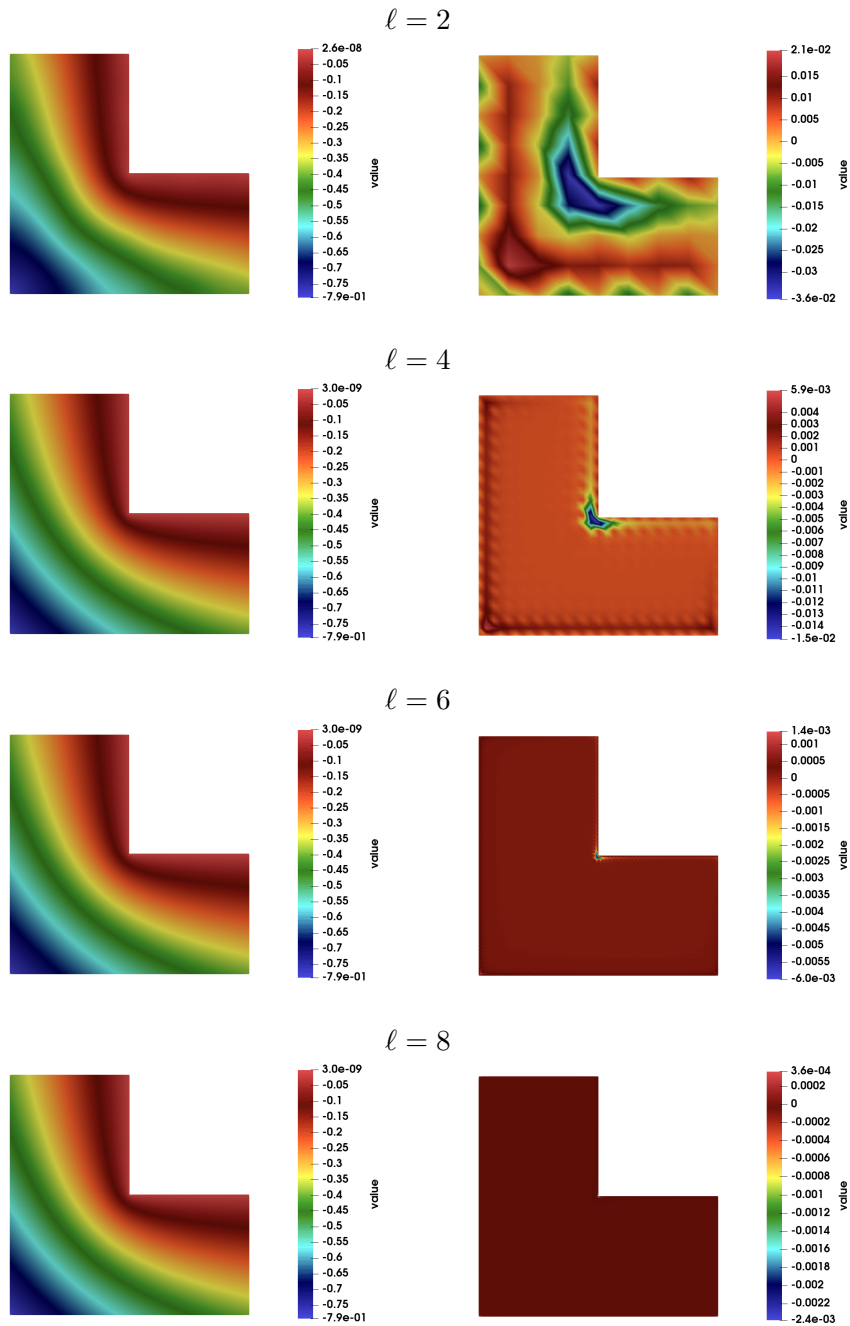


FIGURE 3. Solution (left) and corresponding residuals (right) for the interpolation of the solution to the Laplace equation on the L-shaped domain for levels $\ell = 2, 4, 6, 8$ using $\gamma = 1$ and $\kappa = 10^{-4}$.

6.3. Function on a point cloud in three spatial dimensions. As final example, we consider a function defined on a uniform resampling of the Lucy surface model of the **Stanford 3D Scanning Repository**. To construct the local approximation spaces, we selected random subsamples of the resulting point cloud, ensuring a specific cardinality

for each set. We start with an initial set of 20 points, and at each subsequent level, the cardinality is increased by a factor of 16. In this study, we present results for both nested and non-nested point sets. For the nested case, the indices of the points are randomly shuffled, and subsamples are obtained by selecting the first n points, where n represents the desired cardinality. In contrast, for the non-nested case, each subsample is randomly selected from the entire dataset independently, i.e., without enforcing the inclusion of points from previous levels. Unlike previous tests, this experiment is more general, as the points are not arranged on a uniform grid, they are not necessarily nested, and they are not necessarily quasi-uniform. As test function, we e interpolate

$$f(\mathbf{x}) = \frac{1}{\sqrt[4]{\|\mathbf{x} - \mathbf{x}_0\|_2 + 10^{-4}}}$$

The point \mathbf{x}_0 is selected near the torch that Lucy holds in her left hand. To optimize performance, we use a relatively small value for the parameter γ , reduce the number of vanishing moments, and set a higher a-posteriori threshold. These adjustments help decrease both computational time and the number of non-zero entries. However, a very small γ can compromise the precision, while a very large γ increases the number of conjugate gradient iterations, thereby increasing computational time. A good trade-off is given by $\gamma = 0.2$. Furthermore, we employed a diagonally preconditioned conjugate gradient method with accuracy 10^{-6} to solve the linear system, which reduces the number of iterations by a factor of about three compared to the unpreconditioned case. The number of points per level and the corresponding fill-distances are provided in Table 8.

ℓ	N_ℓ	h (nested)	h (not-nested)
1	20	0.25	0.34
2	320	0.15	0.13
3	5 120	0.061	0.064
4	81 920	0.017	0.018
5	1 310 720	0.0051	0.0050

TABLE 8. Number of points per level and corresponding fill-distances for the interpolation on the Lucy point cloud.

The error is evaluated on a finer set of 2 000 000 points, which are randomly selected once from the original dataset. The evaluation set remains fixed throughout all experiments to ensure consistency in error measurement. The results using the Matérn-1/2 and Matérn-3/2 RBFs are shown in Tables 9 and 10.

We observe that the C^0 -smooth Matérn-1/2 RBF performs better in this scenario, primarily due to the improved conditioning of the associated generalized Vandermonde matrix. In both cases, the approximation error reaches the compression error of 10^{-4} .

A visualization of the solution on all five levels $\ell = 1, \dots, 5$ using the Matérn-1/2 RBF and not-nested points is depicted in Figure 4.

7. CONCLUSION

We have proposed an efficient multiscale approach for scattered data interpolation with globally supported RBFs in combination with the sample matrix compression. In particular, we have extended existing results on the boundedness of the condition numbers of the

$\gamma = 0.2$								
	nested				not-nested			
ℓ	error ₂	order ₂	%nz	CG	error ₂	order ₂	%nz	CG
1	$5.98 \cdot 10^{-1}$	–	50	8	$4.49 \cdot 10^{-1}$	–	50	9
2	$1.60 \cdot 10^{-1}$	2.58	44	26	$1.27 \cdot 10^{-1}$	1.31	42	28
3	$3.08 \cdot 10^{-2}$	1.83	6.5	49	$2.25 \cdot 10^{-2}$	2.44	6.9	45
4	$5.22 \cdot 10^{-3}$	1.39	0.51	56	$2.36 \cdot 10^{-3}$	1.78	0.50	65
5	$7.94 \cdot 10^{-4}$	1.56	0.03	57	$2.51 \cdot 10^{-4}$	1.74	0.03	69

TABLE 9. Results for the interpolation of a test function on the Lucy point cloud for the C^0 -smooth Matérn-1/2 RBF using $\rho = 3$, $q + 1 = 3$, $\kappa = 10^{-4}$ as samplet compression parameters.

$\gamma = 0.2$								
	nested				not-nested			
ℓ	error ₂	order ₂	%nz	CG	error ₂	order ₂	%nz	CG
1	$6.16 \cdot 10^{-1}$	–	50	11	$4.50 \cdot 10^{-1}$	–	50	12
2	$1.48 \cdot 10^{-1}$	2.79	45	74	$1.14 \cdot 10^{-1}$	1.43	44	79
3	$2.92 \cdot 10^{-2}$	1.80	6.5	214	$1.73 \cdot 10^{-2}$	2.66	7.0	247
4	$5.41 \cdot 10^{-3}$	1.32	0.51	341	$1.32 \cdot 10^{-3}$	2.03	0.51	398
5	$8.57 \cdot 10^{-4}$	1.53	0.03	349	$1.61 \cdot 10^{-4}$	1.64	0.03	430

TABLE 10. Results for the interpolation of a test function on the Lucy point cloud for the C^1 -smooth Matérn-3/2 RBF using $\rho = 3$, $q + 1 = 3$, $\kappa = 10^{-4}$ as samplet compression parameters.

generalized Vandermonde matrices within the multiscale approximation towards globally supported RBFs. For appropriately chosen lengthscale parameters, the condition numbers stay independent of the level, which allows for an efficient solution of the resulting linear system by the conjugate gradient method with a bounded number of iterations for a given accuracy. The resulting algorithm has an overall cost of $\mathcal{O}(N \log N)$ for N quasi-uniform data sites, given that the points per level form a geometric sequence. The numerical results demonstrate that the presented approach achieves a similar accuracy to the multiscale approach by compactly supported RBFs, while overcoming previous limitations that made the use of globally supported RBFs impractical for large-scale problems. We have demonstrated that the present multiscale approach can handle datasets with millions of data in both two and three spatial dimensions. As test cases, we have considered smooth and non-smooth data in two dimensions and a complex geometry in three spatial dimensions. In all cases, we achieved accurate results that would have been computationally infeasible without the samplet matrix compression.

Acknowledgement. SA and MM were funded by the SNSF starting grant “Multiresolution methods for unstructured data” (TMSGI2_211684).

REFERENCES

- [1] D. Alm, H. Harbrecht, and U. Krämer. The \mathcal{H}^2 -wavelet method. *J. Comput. Appl. Math.*, 267:131–159, 2014.

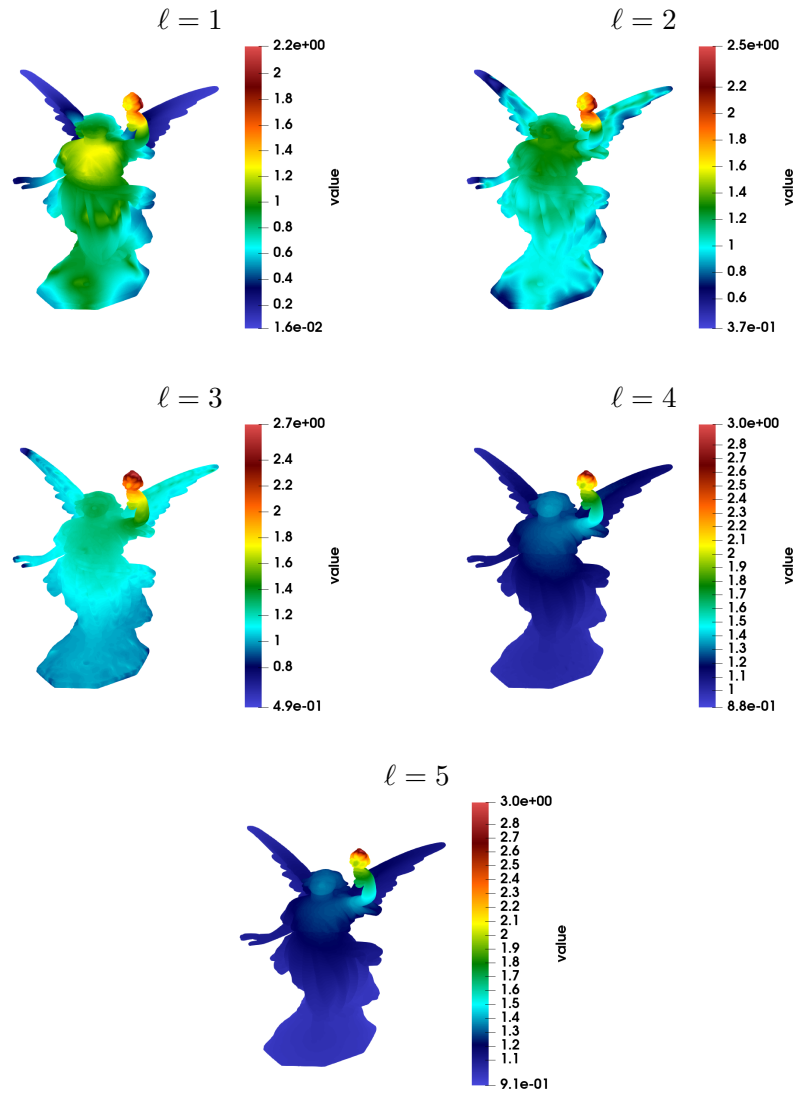


FIGURE 4. Interpolant of the test function on the Lucy point cloud for levels $\ell = 1, \dots, 5$ using the Matérn-1/2 RBF.

- [2] D. Baroli, H. Harbrecht, and Multerer. Samplet basis pursuit: Multiresolution scattered data approximation with sparsity constraints. *IEEE Trans. Sign. Proc.*, 72:1813–1823, 2024.
- [3] M. S. Floater and A. Iske. Multistep scattered data interpolation using compactly supported radial basis functions. *J. Comput. Appl. Math.*, 73(1):65–78, 1996.
- [4] R. Franke. Scattered data interpolation: Tests of some methods. *Math. Comput.*, 38(157):181–200, 1982.
- [5] S. J. Hales and J. Levesley. Error estimates for multilevel approximation using polyharmonic splines. *Numer. Algorithms*, 30(1):1–10, 2002.
- [6] H. Harbrecht, U. Kähler, and R. Schneider. Wavelet galerkin bem on unstructured meshes. *Comput. Vis. Sci.*, 8(3-4):189–199, 2005.
- [7] H. Harbrecht and M. Multerer. Samplets: Construction and scattered data compression. *J. Comput. Phys.*, 471:111616, 2022.
- [8] H. Harbrecht, M. Multerer, O. Schenk, and C. Schwab. Multiresolution kernel matrix algebra. *Numer. Math.*, 156(3):1085–1114, 2024.
- [9] Q. T. Le Gia, I. H. Sloan, and H. Wendland. Multiscale analysis in sobolev spaces on the sphere. *SIAM J. Numer. Anal.*, 48(6):2065–2090, 2010.

- [10] W. R. Madych and S. A. Nelson. Multivariate interpolation: A variational theory, 1983.
- [11] W. R. Madych and S. A. Nelson. Multivariate interpolation and conditionally positive definite functions. II. *Math. Comput.*, 54(189):211–230, 1990.
- [12] B. Matérn. *Spatial variation*, volume 36 of *Lecture Notes in Statistics*. Springer, Berlin, second edition, 1986.
- [13] C. A. Micchelli. *Interpolation of scattered data: Distance matrices and conditionally positive definite functions*. Springer, 1984.
- [14] F. J. Narcowich, R. Schaback, and J. D. Ward. Multilevel interpolation and approximation. *Appl. Comput. Harmon. Anal.*, 7(3):243–261, 1999.
- [15] F. J. Narcowich, N. Sivakumar, and J. D. Ward. On condition numbers associated with radial-function interpolation. *J. Math. Anal. Appl.*, 186(2):457–485, 1994.
- [16] R. Schaback. Error estimates and condition numbers for radial basis function interpolation. *Adv. Comput. Math.*, 3(3):251–264, 1995.
- [17] J. Tausch and J. White. Multiscale bases for the sparse representation of boundary integral operators on complex geometry. *SIAM J. Sci. Comput.*, 24(5):1610–1629, 2003.
- [18] A. Townsend and H. Wendland. Multiscale analysis in sobolev spaces on bounded domains with zero boundary values. *IMA J. Numer. Anal.*, 33(3):1095–1114, 2012.
- [19] H. Wendland. Piecewise polynomial, positive definite and compactly supported radial functions of minimal degree. *Adv. Comput. Math.*, 4:389–396, 1995.
- [20] H. Wendland. *Scattered data approximation*. Cambridge Monographs on Applied and Computational Mathematics. Cambridge University Press, Cambridge, 2004.
- [21] H. Wendland. Multiscale analysis in sobolev spaces on bounded domains. *Numer. Math.*, 116:493–517, 2010.
- [22] H. Wendland. Multiscale radial basis functions. In *Frames and Other Bases in Abstract and Function Spaces: Novel Methods in Harmonic Analysis. Volume 1*, pages 265–299, Cham, 2017. Birkhäuser.
- [23] H. Wendland. *Numerical linear algebra: An introduction*. Cambridge Texts in Applied Mathematics. Cambridge University Press, Cambridge, 2017.
- [24] Z. Wu. Compactly supported positive definite radial functions. *Adv. Comput. Math.*, 4:283–292, 1995.
- [25] Z. Wu and R. Schaback. Local error estimates for radial basis function interpolation of scattered data. *IMA J. Numer. Anal.*, 13(1):13–27, 1993.

SARA AVESANI, ISTITUTO EULERO, USI LUGANO, VIA LA SANTA 1, 6962 LUGANO, SVIZZERA.
Email address: `sara.avesani@usi.ch`

RÜDIGER KEMPF, APPLIED AND NUMERICAL ANALYSIS, DEPARTMENT OF MATHEMATICS, UNIVERSITY OF BAYREUTH, 95440 BAYREUTH, GERMANY
Email address: `ruediger.kempf@uni-bayreuth.de`

MICHAEL MULTERER, ISTITUTO EULERO, USI LUGANO, VIA LA SANTA 1, 6962 LUGANO, SVIZZERA.
Email address: `michael.multerer@usi.ch`

HOLGER WENDLAND, APPLIED AND NUMERICAL ANALYSIS, DEPARTMENT OF MATHEMATICS, UNIVERSITY OF BAYREUTH, 95440 BAYREUTH, GERMANY
Email address: `holger.wendland@uni-bayreuth.de`